High-order time-splitting Hermite and Fourier spectral methods for the Gross-Pitaevskii equation

Mechthild Thalhammer [b,*], Marco Caliari [a], Christof Neuhauser [b]

[a] *Dipartimento di Informatica, Università degli Studi di Verona, Ca' Vignal 2, Strada Le Grazie 15, I-37134 Verona, Italy*
[b] *Institut für Mathematik, Leopold-Franzens Universität Innsbruck, Technikerstraße 13/7, A-6020 Innsbruck, Austria*

ARTICLE INFO

Keywords:
Nonlinear Schrödinger equations
Gross–Pitaevskii equation
Pseudospectral methods
Exponential operator splitting methods

ABSTRACT

In this paper, we are concerned with the numerical solution of the time-dependent Gross–Pitaevskii Equation (GPE) involving a quasi-harmonic potential. Primarily, we consider discretisations that are based on spectral methods in space and higher-order exponential operator splitting methods in time. The resulting methods are favourable in view of accuracy and efficiency; moreover, geometric properties of the equation such as particle number and energy conservation are well captured.

Regarding the spatial discretisation of the GPE, we consider two approaches. In the unbounded domain, we employ a spectral decomposition of the solution into Hermite basis functions; on the other hand, restricting the equation to a sufficiently large bounded domain, Fourier techniques are applicable. For the time integration of the GPE, we study various exponential operator splitting methods of convergence orders two, four, and six.

Our main objective is to provide accuracy and efficiency comparisons of exponential operator splitting Fourier and Hermite pseudospectral methods for the time evolution of the GPE. Furthermore, we illustrate the effectiveness of higher-order time-splitting methods compared to standard integrators in a long-term integration.

1. Introduction

In the present paper, we are concerned with the numerical solution of the *time-dependent Gross–Pitaevskii Equation* (GPE) [14,21]

$$\mathrm{i}\hbar\partial_t\psi(x,t) = (-\tfrac{\hbar^2}{2m}\Delta + V(x) + g|\psi(x,t)|^2)\psi(x,t), \tag{1}$$

describing the wave function $\psi : \mathbb{R}^d \times \mathbb{R}_{\geqslant 0} \to \mathbb{C}$ of a *Bose–Einstein condensate*. Our main objective is to compare space and time discretisations that are based on Hermite and Fourier spectral methods and exponential splitting methods of orders two, four, and six; moreover, we illustrate the effectiveness of higher-order splitting methods compared to standard integrators in a long-term integration. In most cases, we use the ground state of the GPE as a reliable reference solution, computed by employing the Hermite spectral decomposition and directly minimising the energy functional, see [3,8].

Over the past years, numerous works were devoted to the discretisation of nonlinear Schrödinger equations; we mention [1,2,4,10,11,20,24,25], where a particular emphasis is given to accuracy and the preservation of geometric properties. For the spatial discretisation of the GPE, Hermite pseudospectral methods are used in [2,11]; on the other hand, restricting the

* Corresponding author.
E-mail address: mechthild.thalhammer@uibk.ac.at (M. Thalhammer).

problem to a bounded domain, Fourier spectral methods are applicable, see Bao et al. [1]. The favourable behaviour of the second-order Strang splitting and a fourth-order time-splitting scheme regarding accuracy, efficiency, and the conservation of geometric properties is illustrated in [1,2]. For the cubic Schrödinger equation, numerical comparisons of different space and time discretisations are provided by Pérez–García and Liu [20].

The present work is organised as follows. In Section 2, we restate the time-dependent d-dimensional GPE in a normalised form. Further, we briefly discuss the special case of a harmonic potential and vanishing interaction that leads to the time-dependent linear Schrödinger equation; in this situation, the ground and the excited states are given by the Hermite functions. The linear Schrödinger equation also motivates the consideration of a Hermite spectral decomposition for the nonlinear GPE. Sections 3 and 4 are devoted to numerical discretisations of the GPE based on Hermite and Fourier spectral methods in space and exponential operator splitting methods in time; we note that an extension to systems of coupled GPEs is straightforward, see also Caliari et al. [8]. In Section 5, we present several illustrations regarding accuracy, efficiency, and the preservation of geometric properties. The numerical experiments are carried out for problems in two space dimensions; however, in view of the tensor product structure of the spatial discretisation, we expect our conclusions to be maintained in three space dimensions as well. In Section 6, we finally summarise our results and discuss open questions.

The following notations are tacitly employed throughout. For a multi-index of integer numbers $m = (m_1, m_2, \dots, m_d) \in \mathbb{Z}^d$, the relation $\leqslant$ is understood componentwise. For an element $x = (x_1, x_2, \dots, x_d) \in \mathbb{R}^d$, we denote by $|x|$ its Euclidean norm. As usual, the d-dimensional Laplacian is defined through $\Delta = \partial^2_{x_1} + \cdots + \partial^2_{x_d}$. The Lebesgue space $L^2(\Omega^d)$ of square integrable complex-valued functions on $\Omega^d \subseteq \mathbb{R}^d$ is endowed with scalar product $(\cdot|\cdot)_{L^2(\Omega^d)}$ and associated norm $\|\cdot\|_{L^2(\Omega^d)}$ defined by

$$(f|g)_{L^2(\Omega^d)} = \int_{\Omega^d} f(x)\overline{g(x)}\mathrm{d}x, \quad \|f\|_{L^2(\Omega^d)} = \sqrt{(f|f)_{L^2(\Omega^d)}}, \quad f, g \in L^2(\Omega^d);$$

for notational simplicity, we omit the domain in the scalar product and norm.

2. Gross–Pitaevskii equation

In the present section, we state a normalisation of the d-dimensional GPE (1) that is obtained by a linear transformation of the spatial variable and a rescaling of the wave function, see also Caliari et al. [8]; moreover, we introduce the ground and excited state solutions of the GPE by means of a nonlinear eigenvalue problem. Existence and uniqueness results for time-dependent Schrödinger equations are found in Cazenave [9, Chapters 4 and 6].

2.1. Time-dependent Gross–Pitaevskii equation

Henceforth, we consider the following normalisation of the time-dependent Gross–Pitaevskii equation (GPE):

$$\mathrm{i}\partial_t \psi(x,t) = (-\tfrac{1}{2}\Delta + V(x) + \vartheta|\psi(x,t)|^2)\psi(x,t), \quad t \geqslant 0; \tag{2a}$$

the equation is subject to asymptotic boundary conditions on the unbounded spatial domain $\mathbb{R}^d$, i.e., we require $\psi(x,t) \to 0$ as $|x| \to \infty$. Without any loss of generality, we further suppose the initial value $\psi(\cdot,0) \in L^2(\mathbb{R}^d)$ to satisfy the normalisation condition

$$\|\psi(\cdot,0)\|^2_{L^2} = 1. \tag{2b}$$

In the present paper, we restrict ourselves to the case of a scaled harmonic potential $V = \frac{1}{2}V_{\mathrm{H}}$ where

$$V_{\mathrm{H}}(x) = \sum_{j=1}^{d} \gamma_j^4 x_j^2, \quad \gamma_j > 0, \quad 1 \leqslant j \leqslant d; \tag{2c}$$

however, as indicated in Section 4, our approach extends to more general real-valued potentials V. Also, we assume the *coupling constant* ϑ to be non-negative, that is, we restrict ourselves to a *defocusing* condensate.

As proven in Cazenave [9, Thm 4.1.1], a fundamental property of (2) is the preservation of the *particle number*

$$\|\psi(\cdot,t)\|^2_{L^2} = \|\psi(\cdot,0)\|^2_{L^2} = 1, \quad t \geqslant 0, \tag{3a}$$

see (2b). Moreover, the *energy functional*

$$E(\psi(\cdot,t)) = ((-\tfrac{1}{2}\Delta + V + \tfrac{1}{2}\vartheta|\psi(\cdot,t)|^2)\psi(\cdot,t)|\psi(\cdot,t))_{L^2} \tag{3b}$$

is time-independent, that is, it holds $E(\psi(\cdot,t)) = E(\psi(\cdot,0))$ for $t \geqslant 0$; we further require $E(\psi(\cdot,0)) < \infty$.

2.2. Ground and excited states

The *ground state solution* of the GPE (2) is a solution of the form

$$\psi(x,t) = \mathrm{e}^{-\mathrm{i}\mu t}\phi(x), \quad x \in \mathbb{R}^d, \quad t \geqslant 0, \tag{4a}$$

with $\mu \in \mathbb{R}$ and ϕ a real-valued (positive) function that minimises the energy functional $E(\psi(\cdot,t)) = E(\phi)$, see (3b). Inserting (4a) into (2a) and using (3a) yields

$$(-\tfrac{1}{2}\Delta + V + \vartheta\phi^2)\phi = \mu\phi, \quad \mu = E(\phi) + \tfrac{1}{2}\vartheta(\phi^3|\phi)_{L^2}. \tag{4b}$$

Further solutions of the GPE (2) that allow a decomposition (4a) and thus solve the nonlinear eigenvalue problem (4b) are called *excited state solutions*.

We next consider the special case where the parameter ϑ vanishes and the potential V is given by the scaled harmonic potential V_{H}, see (2c). In this situation, the GPE (2) reduces to the *linear Schrödinger equation*

$$\mathrm{i}\partial_t\psi(x,t) = \tfrac{1}{2}(-\Delta + V_H(x))\psi(x,t), \quad t \geqslant 0,$$

and, as well known, the *Hermite functions* with associated eigenvalues

$$\mathscr{H}_m(x) = \prod_{j=1}^{d}\left(H_{m_j}(x_j)\mathrm{e}^{-\frac{1}{2}(\gamma_j x_j)^2}\right), \quad \lambda_m = \sum_{j=1}^{d}\gamma_j^2\left(m_j + \frac{1}{2}\right), \tag{5a}$$

solve (4b) for $\vartheta = 0$, that is, for any $m \geqslant 0$ it holds

$$\tfrac{1}{2}(-\Delta + V_H)\mathscr{H}_m = \lambda_m\mathscr{H}_m; \tag{5b}$$

here, we let H_{m_j} denote the *Hermite polynomial* of degree m_j, normalised with respect to the weight function $w_j(x_j) = \mathrm{e}^{-(\gamma_j x_j)^2}$. The Hermite functions $(\mathscr{H}_m)$ form an orthonormal basis of the function space $L^2(\mathbb{R}^d)$; in particular, it holds $(\mathscr{H}_k|\mathscr{H}_m)_{L^2} = \delta_{km}$ with Kronecker delta δ_{km}.

3. Pseudospectral methods

In the following, we discuss two approaches for the spatial discretisation of the GPE that are based on Hermite and Fourier spectral decompositions of the solution, respectively.

3.1. Hermite pseudospectral method

In this section, we let $m \in \mathbb{Z}^d$ be a multi-index with non-negative components, i.e., we suppose $m \geqslant 0$; hence, for a family (a_m) we write

$$\sum_m a_m = \sum_{m\geqslant 0} a_m$$

for short. Using that the Hermite functions $(\mathscr{H}_m)$ form an orthonormal basis of the function space $L^2(\mathbb{R}^d)$, the representation

$$\psi(\cdot,t) = \sum_m \psi_m(t)\mathscr{H}_m, \quad \psi_m(t) = (\psi(\cdot,t)|\mathscr{H}_m)_{L^2}, \tag{6a}$$

follows, see also Section 2.2; besides, due to Parseval's equality, the identity

$$\|\psi(\cdot,t)\|_{L^2}^2 = \sum_m |\psi_m(t)|^2 \tag{6b}$$

is valid. Truncating the infinite sum in (6a) yields

$$\psi_M(\cdot,t) = \sum\nolimits_M \psi_m(t)\mathscr{H}_m = \sum_{m\leqslant M-1}\psi_m(t)\mathscr{H}_m \tag{7a}$$

with coefficient vector $\psi(t) = (\psi_m(t))_{m\leqslant M-1}$ given by (6a); the above relation (6b) implies

$$\|\psi_M(\cdot,t)\|_{L^2}^2 = |\psi(t)|^2 = \sum\nolimits_M |\psi_m(t)|^2. \tag{7b}$$

Results on the approximation error of the Hermite spectral method are found in Boyd [6, Chapter 17.4]. For computing numerically the coefficients $\psi_m(t)$ given by (6a), we apply the following approximation:

$$\psi_m(t) = \int_{\mathbb{R}^d}\psi(x,t)\mathscr{H}_m(x)\mathrm{d}x \approx \sum\nolimits_M \omega_k\mathrm{e}^{|\xi_k|^2}\psi(\xi_k,t)\mathscr{H}_m(\xi_k) \tag{8}$$

with $\xi_k = (\xi_{k_1}, \ldots, \xi_{k_d})$ and $\omega_k = \omega_{k_1} \cdot \ldots \cdot \omega_{k_d}$; here, ξ_{k_j} and ω_{k_j} denote the nodes and weights of the Gauss–Hermite quadrature formula relative to $w_j(x_j) = \mathrm{e}^{-(\gamma_j x_j)^2}$.

3.2. Fourier pseudospectral method

In order to apply Fourier techniques for the spatial discretisation of (2), we restrict the unbounded domain to a bounded set Ω^d; for simplicity, we assume $\Omega = [-a, a]$ to be a symmetric interval with $a > 0$ chosen sufficiently large. For the remainder of this section, we denote by $m \in \mathbb{Z}^d$ a multi-index of integer numbers; the Lebesgue space $L^2(\Omega^d)$ is endowed with the scalar product

$$(f|g)_{L^2} = \int_{\Omega^d} f(x)\overline{g(x)}\mathrm{d}x, \quad f, g \in L^2(\Omega^d),$$

and corresponding norm. In contrast to (5b), we now employ the eigenvalue decomposition

$$-\tfrac{1}{2}\Delta\mathscr{F}_m = \lambda_m \mathscr{F}_m$$

involving the *Fourier basis functions* $(\mathscr{F}_m)$ and associated eigenvalues (λ_m) that are given by

$$\mathscr{F}_m(x) = \prod_{j=1}^{d} F_{m_j}(x_j), \quad F_{m_j}(x) = \tfrac{1}{\sqrt{2a}}\mathrm{e}^{\mathrm{i}m_j\pi\left(\frac{1}{a}x+1\right)}, \quad \lambda_m = \tfrac{1}{2a^2}\pi^2\sum_{j=1}^{d} m_j^2;$$

in particular, it holds $(\mathscr{F}_k|\mathscr{F}_m)_{L^2} = \delta_{km}$. Therefore, similarly to (6a), the representation

$$\psi(\cdot, t) = \sum_m \psi_m(t)\mathscr{F}_m, \quad \psi_m(t) = (\psi(\cdot, t)|\mathscr{F}_m)_{L^2}, \tag{9}$$

follows for elements in $L^2(\Omega^d)$; as before, the coefficients $(\psi_m(t))$ satisfy (6b). For some integer $M_1 \geqslant 0$ we henceforth set $M = 2M_1$. Truncating the infinite sum in (9) yields

$$\psi_M(\cdot, t) = \sum_{m}{}_M \psi_m(t)\mathscr{F}_m = \sum_{-M_1 \leqslant m \leqslant M_1 - 1} \psi_m(t)\mathscr{F}_m; \tag{10}$$

the coefficient vector $\psi(t) = (\psi_m(t))_{-M_1 \leqslant m \leqslant M_1 - 1}$ fulfills relation (7b). Results on the favourable approximation behaviour of the Fourier spectral method are found in Boyd [6, Chapter 2]. For computing numerically the coefficients $\psi_m(t)$ given by (9), we apply the trapezoidal rule

$$\psi_m(t) = \int_{\Omega^d} \psi(x, t)\mathscr{F}_m(x)\mathrm{d}x \approx \omega \sum_k{}_M \psi(\xi_k, t)\mathscr{F}_m(\xi_k); \tag{11}$$

here, we set $\xi_k = (\xi_{k_1}, \ldots, \xi_{k_d})$ with equidistant grid points $\xi_{k_j} = \frac{1}{M_1}ak_j$ and further $\omega = (\frac{1}{M_1}a)^d$.

4. Time-splitting methods

In this section, we introduce exponential operator splitting methods for the time integration of evolutionary nonlinear Schrödinger equations such as (2). For a detailed treatment of splitting and composition methods for ordinary differential equations, we refer to [15,19]. In particular for the GPE, the favourable behaviour of a second-order Strang type splitting and a fourth-order splitting scheme regarding accuracy, efficiency, and the preservation of geometric properties is confirmed by numerical experiments given in [1,2]; a convergence analysis for Strang type splitting methods is provided by Caliari et al. [7], see also Lubich [17].

In order to state the considered numerical method class, it is convenient to formulate the partial differential equation (2a) as an abstract ordinary differential equation; more precisely, suppressing the spatial variable in the equation and setting $u(t) = \psi(\cdot, t)$, we obtain an initial value problem of the form

$$u'(t) = \Big(A + B(u(t))\Big)u(t), \quad t \geqslant 0, \quad u(0) \text{ given}. \tag{12}$$

Exponential operator splitting methods rely on a decomposition of the right-hand side of the differential equation into two parts in such a way that the resulting differential equations

$$v'(t) = Av(t), \quad t \geqslant 0, \quad v(0) \text{ given}, \tag{13a}$$
$$w'(t) = B(w(t))w(t), \quad t \geqslant 0, \quad w(0) \text{ given}, \tag{13b}$$

are solvable in a favourable way. Regarding the Hermite and Fourier pseudospectral methods, we distinguish the following approaches:

$$\text{Hermite}: \quad A = \tfrac{1}{2}\mathrm{i}(\Delta - V_{\mathrm{H}}), \quad B(u(t)) = -\mathrm{i}\Big(V - V_{\mathrm{H}} + \vartheta|u(t)|^2\Big),$$
$$\text{Fourier}: \quad A = \tfrac{1}{2}\mathrm{i}\Delta, \quad B(u(t)) = -\mathrm{i}\Big(V + \vartheta|u(t)|^2\Big),$$

see also (2).

On the one hand, the solution of the initial value problem (13a) equals

$$v(t) = \mathrm{e}^{tA} v(0), \quad t \geqslant 0. \tag{14a}$$

The evaluation of v relies on the representation of the initial value with respect to the Hermite and Fourier basis functions, see Section 3; more precisely, provided that $v(0)$ can be decomposed into the basis functions $(\mathscr{B}_m)$, where $\mathscr{B}_m = \mathscr{H}_m$ or $\mathscr{B}_m = \mathscr{F}_m$, respectively, the exact solution value at time $t \geqslant 0$ is given by

$$v(t) = \sum_m v_m \mathrm{e}^{-\mathrm{i}t\lambda_m} \mathscr{B}_m, \quad t \geqslant 0, \quad v(0) = \sum_m v_m \mathscr{B}_m. \tag{14b}$$

For the numerical evaluation of $v(t)$, we collocate (13a) at the nodes (ξ_k) and approximate the coefficients (v_m) by means of the Gauss–Hermite or the trapezoid quadrature formula, respectively, see (8) and (11). Clearly, the numerical approximation to $v(t)$ can be evaluated at any x; however, much less computational effort is required when $v(t)$ is evaluated numerically at the quadrature nodes. In fact, for the Hermite pseudospectral method the values $\mathscr{H}_m(\xi_k)$ can be stored; for the Fourier pseudospectral method the Fast Fourier Transform is applicable. On the other hand, regarding the initial value problem (13b), the exact solution is available; namely, due to the fact that the differential equation for w leaves $|w(t)|$ invariant, it follows $B(w(t)) = B(w(0))$ and thus

$$w(t) = \mathrm{e}^{tB(w(0))} w(0), \quad t \geqslant 0, \tag{14c}$$

see also Caliari et al. [7]. In the numerical computation, we again collocate the equation at the quadrature nodes (ξ_k); then, the approximate solution is obtained by a rapid componentwise multiplication.

The basic idea of exponential operator splitting methods is to compose the solutions of (13) in a suitable way. A widely used scheme is based on the second-order Strang [22] or *symmetric Trotter* [27] splitting; for a step size $h > 0$ and an initial value $u_0 \approx u(0)$, approximations u_n to the exact solution values $u(nh)$, $n \geqslant 0$, are given by the recurrence formula

$$u_n = \mathrm{e}^{\frac{1}{2}hB(U_n)} U_n, \quad U_n = \mathrm{e}^{hA} \mathrm{e}^{\frac{1}{2}hB(u_{n-1})} u_{n-1}, \quad \text{or} \tag{15a}$$

$$u_n = \mathrm{e}^{\frac{1}{2}hA} \mathrm{e}^{\frac{1}{2}hB(U_n)} U_n, \quad U_n = \mathrm{e}^{\frac{1}{2}hA} u_{n-1}, \tag{15b}$$

respectively. We note that for the Fourier spectral method the solution (14a) satisfies the periodic boundary conditions imposed implicitly by the spectral approximation; therefore, this is also true for the auxiliary stage U_n and the numerical solution value u_n in (15b).

Higher-order exponential operator splitting methods for (12) can be cast into the following form:

$$\begin{aligned} u_n &= \mathrm{e}^{b_s hB(U_{n,s})} U_{n,s}, \\ U_{n,1} &= \mathrm{e}^{a_1 hA} u_{n-1}, \quad U_{n,\,j} = \mathrm{e}^{a_j hA} \mathrm{e}^{b_{j-1} hB(U_{n,\,j-1})} U_{n,\,j-1}, \quad 2 \leqslant j \leqslant s, \end{aligned} \tag{16}$$

with real coefficients $a_j, b_j \in \mathbb{R}$, $1 \leqslant j \leqslant s$. Example methods were proposed in [5,16,18,23,28], e.g. see also [15,19]. In Section 5, we include numerical experiments for the splitting schemes of orders two, four, and six, respectively, that are collected in Table 1.

As shown in Thalhammer [26], any splitting method retains its classical convergence order for time-dependent *linear* Schrödinger equations, provided that the initial value and the potential fulfill suitable regularity requirements. The numerical experiments presented in Section 5.2 and the theoretical analysis for the second-order Strang type splitting (15) given in [7,17] indicate that this result is also true for nonlinear Schrödinger equations with sufficiently regular solutions; however, extending the convergence analysis to general exponential operator splitting methods is out of the scope of the present work.

Table 1
Exponential operator splitting methods of order p involving s compositions.

Method		Order	#Compositions
McLachlan	McLachlan [15, V. 3.1, (3.3), pp. 138–139]	$p = 2$	$s = 3$
Strang	Strang (15a)	$p = 2$	$s = 2$
BM4-1	Blanes and Moan [5, Table 2, PRKS_6]	$p = 4$	$s = 7$
BM4-2	Blanes and Moan [5, Table 3, SRKN_6^b]	$p = 4$	$s = 7$
M4	McLachlan [15, V. 3.1, (3.6), p. 140]	$p = 4$	$s = 6$
S4	Suzuki [15, II. 4, (4.5), p. 41]	$p = 4$	$s = 6$
Y4	Yoshida [15, II. 4, (4.4), p. 40]	$p = 4$	$s = 4$
BM6-1	Blanes and Moan [5, Table 2, PRKS_{10}]	$p = 6$	$s = 11$
BM6-2	Blanes and Moan [5, Table 3, SRKN_{11}^b]	$p = 6$	$s = 12$
BM6-3	Blanes and Moan [5, Table 3, SRKN_{14}^a]	$p = 6$	$s = 15$
KL6	Kahan and Li [15, V. 3.2, (3.12), pp. 144]	$p = 6$	$s = 10$
S6	Suzuki [15, II. 4, (4.5), pp. 41]	$p = 6$	$s = 26$
Y6	Yoshida [15, V. 3.2, (3.11), pp. 144]	$p = 6$	$s = 8$

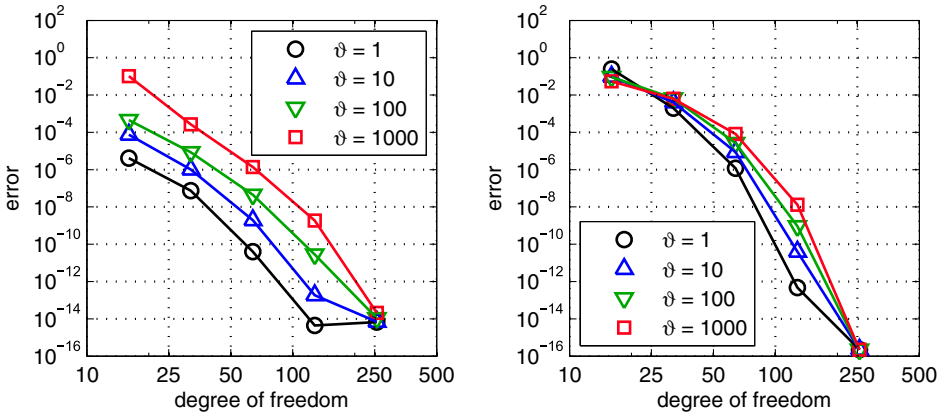

Fig. 1. Spatial error of the Hermite (left picture) and Fourier (right picture) spectral method.

We finally note that the total particle number (3a) is preserved by exponential operator splitting methods (16) applied to the GPE (2); this follows from the conservation of the L^2-norm when solving the differential equations in (13).

5. Numerical experiments

In this section, we present several numerical experiments comparing time-splitting spectral methods when applied to the two-dimensional GPE (2) involving a harmonic potential. Our experiments mainly rely on the computation of the ground state and its propagation, see Caliari et al. [8]. Consequently, making use of the fact that the solutions are even functions, it would be possible to reduce the number of required basis functions for the Hermite and Fourier spectral methods; however, in our presentation, we did not take into account this reduction. For the Fourier spectral method, we henceforth set $\Omega = [-15, 15]$.

The numerical experiments were implemented in MATLAB; the code is available from the authors on request. In the Hermite case, we compute and store once and for all the values $\mathscr{H}_m(\xi_k)$; in two space dimensions, it is then possible to evaluate each of the double sums in (7a) and (8) by two matrix–matrix multiplications at a cost of $\mathcal{O}(M^3)$. For the Fourier transforms (10) and (11) the MATLAB–functions `ifft2` and `fft2` of cost $\mathcal{O}(M^2 \log M)$ are used. The long-term computations were carried out on the Opteron cluster.[1] of the High Performance Computing Consortium at the University of Innsbruck.

5.1. Spatial error

In order to illustrate the accuracy of the Hermite and Fourier spectral methods, we use the ground state solution of the two-dimensional GPE (2) computed with 256×256 degrees of freedom as reference solution ψ, see (4a); we choose $V(x) = V_{\mathrm{H}}(x) = \frac{1}{2}(x_1^2 + x_2^2)$. For the Hermite spectral method, we evaluate $\psi(x, 0)$ at the Gauss–Hermite quadrature points corresponding to $M = 2^i$, $4 \leqslant i \leqslant 8$. We then compute an approximation $\widetilde{\psi}_M(x, 0)$ to $\psi_M(x, 0)$ by means of (7a), where the spectral coefficients are obtained from (8). Finally, the difference $\|\psi_M(\cdot, 0) - \psi(\cdot, 0)\|_{L^2}$ is computed through (7b). The same approach is employed for the Fourier spectral method. First, the reference solution $\psi(x, 0)$ is evaluated at 256×256 equidistant grid points in the square $[-15, 15] \times [-15, 15]$; then, an approximation corresponding to $M = 2^i$, $4 \leqslant i \leqslant 8$, is determined by (10) and (11), and, finally, the error is computed through (7b).

The results displayed in Fig. 1 show that for $M \leqslant 128$ and $\vartheta \leqslant 100$ the Hermite spectral error is smaller than the Fourier spectral error. Further, for the Hermite spectral method it is possible to retain the original solution only up to a *Hermite transform* error of about 10^{-14}, even using the same degree of freedom 256×256, whereas the *Fourier transform* error is of the magnitude of the machine precision.

The Gauss–Hermite quadrature nodes and weights are obtained as solutions of an eigenvalue problem, see Gautschi [12,13] and references therein; furthermore, the Hermite functions are computed through a recurrence relation. Numerical experiments showed that it would be possible to reduce the Hermite transform error by using *variable precision arithmetic* for the computation of the quadrature nodes and weights; however, due to the additional computational effort required, we did not further exploit this approach.

We finally note that the artificial boundary conditions introduced by the Fourier spectral method seem to have no effect on the approximation of the ground state.

[1] See http://unix-docu.uibk.ac.at/zid/systeme/unix-hosts/hc-cluster/.

5.2. Temporal order

We next determine the convergence orders of various exponential operator splitting methods listed in Table 1 when applied to the two-dimensional GPE (2) with harmonic potential $V(x) = V_{\mathrm{H}}(x)$.

To this purpose, we consider the time evolution of the ground state $\psi(x,0)$ up to a final time $T = 1$, see also (4a). First of all, we verified the reliability of our code comparing the two numerical reference solutions obtained for 128×128 Hermite and Fourier basis functions, respectively, and the time step size $h = 2^{-11}$ with the exact solution given by $\psi(x,T) = \mathrm{e}^{-\mathrm{i}\mu T}\psi(x,0)$. We then computed the temporal convergence orders in a standard way for different time step sizes ranging from 2^{-9} to 1. An accuracy comparison of different time-splitting spectral methods with respect to a common reference solution will be given in Section 5.3.

The results obtained for $\vartheta = 1$ and $\vartheta = 100$, respectively, are displayed in Figs. 2 and 3; the slope of the dashed-dotted line reflects the expected classical order. We refer to the fourth- and sixth-order splitting schemes by the initials of the authors and their orders of convergence, see also Table 1. In particular, the partitioned Runge–Kutta methods PRKS_6 and PRKS_{10} as well as the Runge–Kutta–Nyström methods SRKN_6^b, SRKN_{11}^b, and SRKN_{14}^a by Blanes and Moan [5, Tables 2 and 3] are denoted by BM4-1, BM6-1 and BM4-2, BM6-2, BM6-3, respectively; we note that the schemes SRKN_6^b (BM4-2) and SRKN_{14}^a (BM6-3) are claimed to be favourable in view of their small error constants.

The Hermite and Fourier space discretisations show a similar behaviour. As expected, for $\vartheta = 1$ the temporal convergence order is clearly obtained for each splitting method. As soon as the nonlinear part increases, i.e. for $\vartheta = 100$, the error increases; furthermore deflections in the temporal order might occur for larger time step sizes.

In order to illustrate the efficiency of the considered splitting methods, we further include the temporal error versus the total number of the spectral transformations reflecting the principal computational cost in the time integration, see Figs. 4 and 5; the displayed results confirm the favourable behaviour of the schemes BM4-2 and BM6-3. Although the cost of the Fast Fourier Transform in two space dimensions is $\mathcal{O}(M^2 \log M)$ compared with a cost of $\mathcal{O}(M^3)$ for the Hermite transform, in the present situation, for values $M \leqslant 128$, the latter turns out to be comparable or even faster; this behaviour is well known, see Boyd [6, Chapter 10] and also observed in Fig. 6 (right picture), where the mean computational cost of a single spectral transform in two space dimensions is given.

5.3. Long-term integration

In order to illustrate the effectiveness of higher-order time-splitting Fourier and Hermite spectral methods in long-term integrations, we consider the two-dimensional time-dependent GPE (2) with harmonic potential $V(x) = 2V_{\mathrm{H}}(x)$ and $\vartheta = 1$ on the time interval $[0,T]$ where $T = 400$; as initial value we choose the ground state of the GPE with harmonic potential

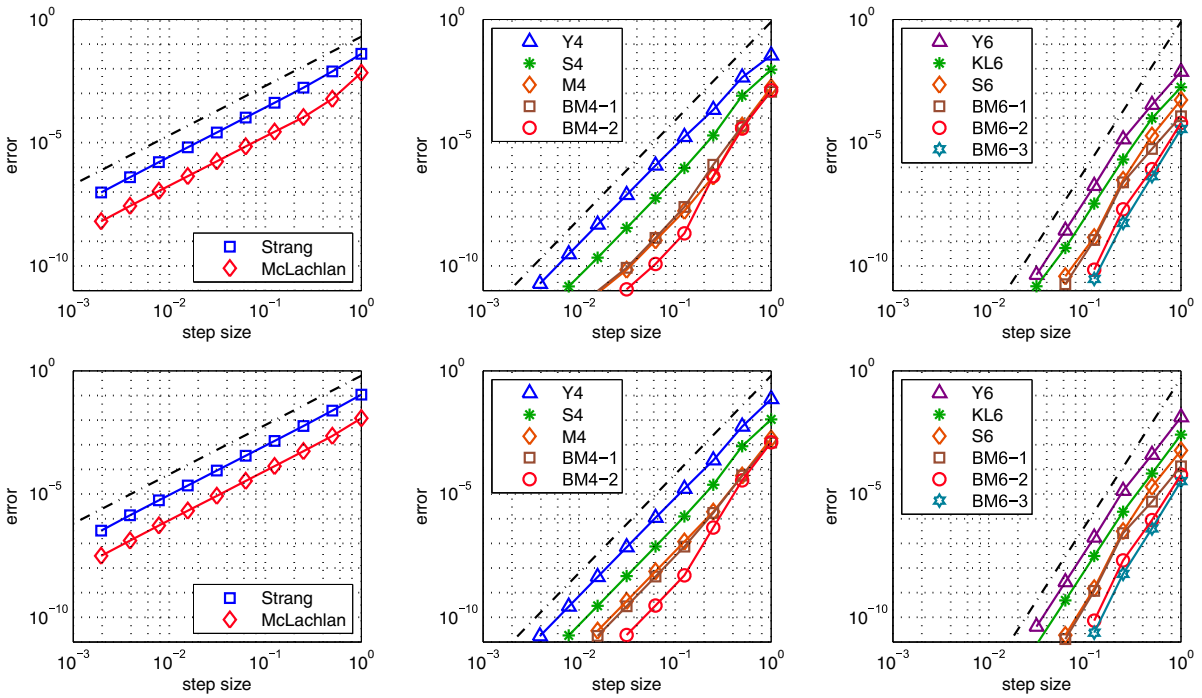

Fig. 2. Temporal orders of various time-splitting Hermite (first row) and Fourier (second row) spectral methods when applied to the two-dimensional GPE (2) with $\vartheta = 1$.

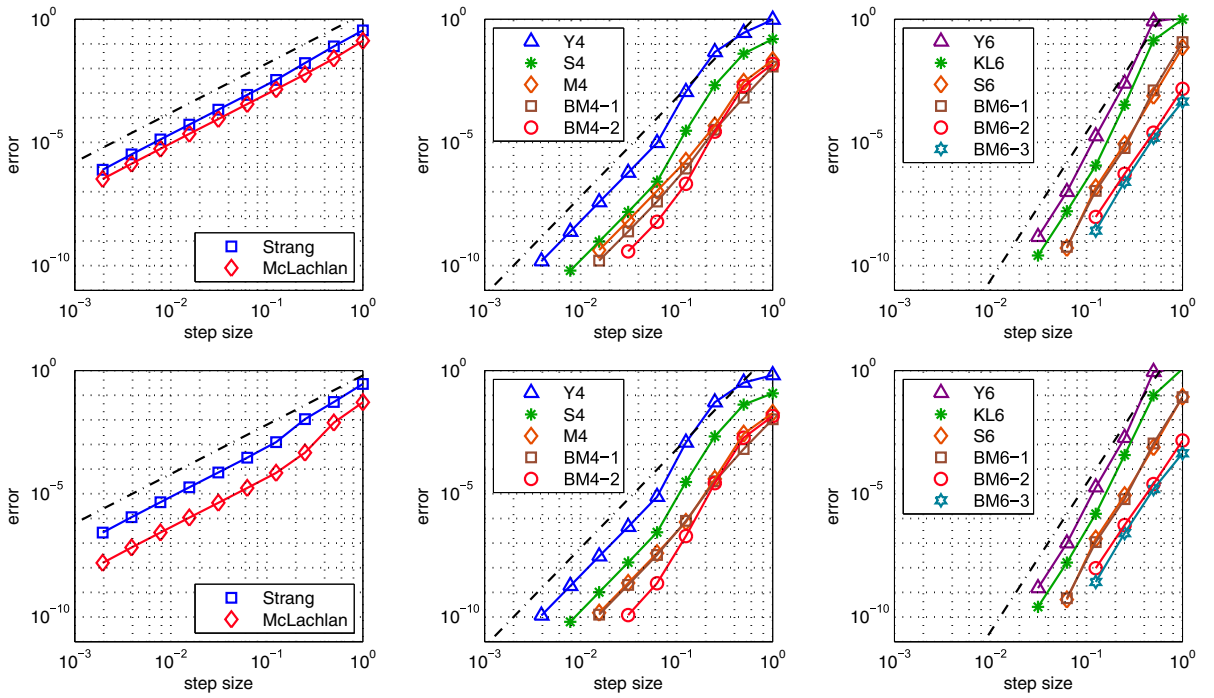

Fig. 3. Temporal orders of various time-splitting Hermite (first row) and Fourier (second row) spectral methods when applied to the two-dimensional GPE (2) with $\vartheta = 100$.

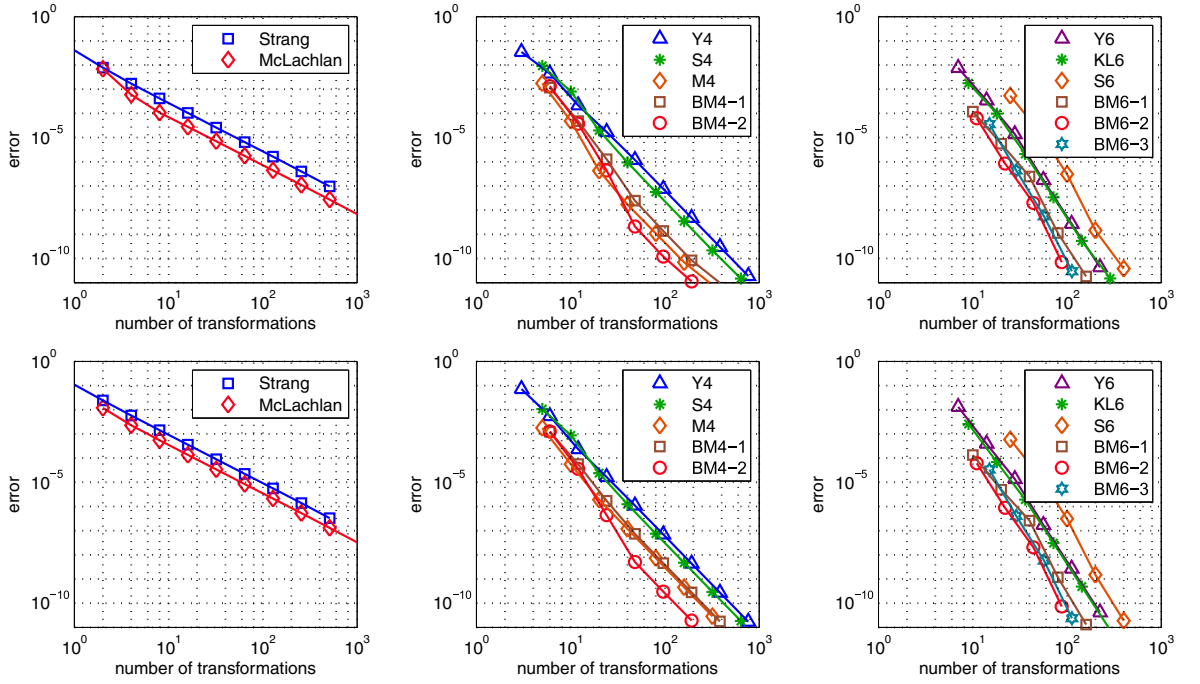

Fig. 4. Efficiency of various time-splitting Hermite (first row) and Fourier (second row) spectral methods when applied to the two-dimensional GPE (2) with $\vartheta = 1$.

$V(x) = V_{\mathrm{H}}(x)$ at $t = 0$. Following Dion and Cancès [11] we call this experiment *breathing*; for $0 \leqslant t \leqslant 13$ the solution is displayed in Fig. 7.

Among the previously considered time-splitting methods, we select the widely used Strang splitting as well as the methods SRKN_6^b (BM4-2) and SRKN_{14}^a (BM6-3) by Blanes and Moan [5]. A reference solution is computed by means of the scheme

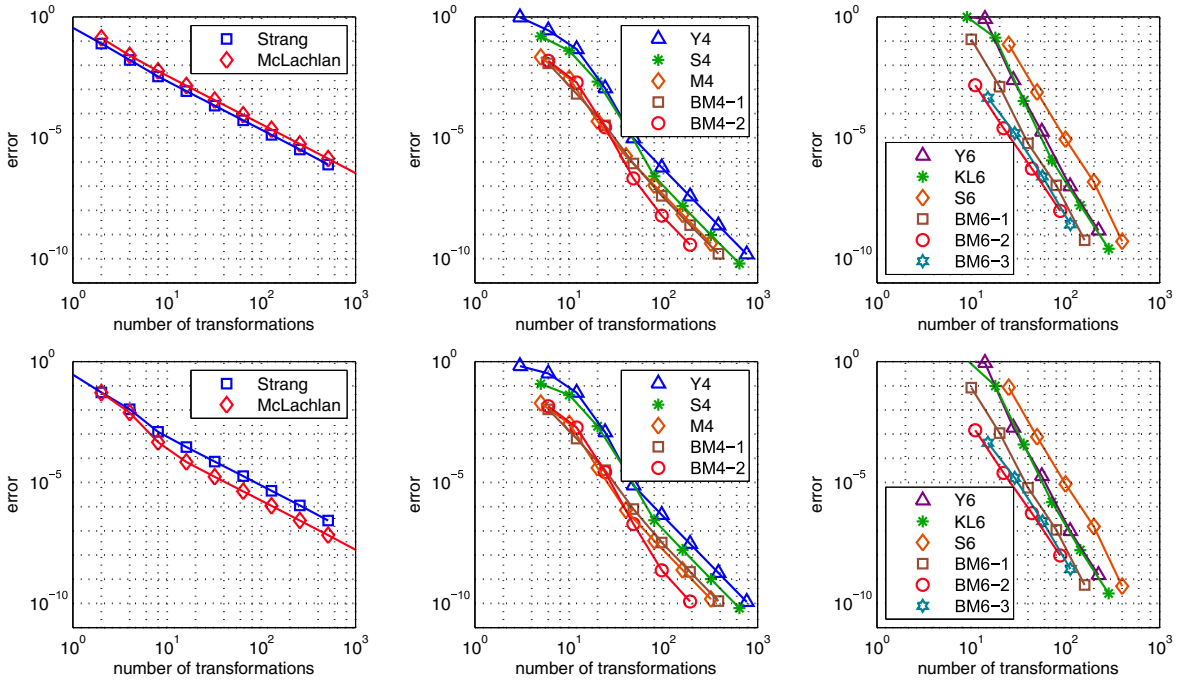

Fig. 5. Efficiency of various time-splitting Hermite (first row) and Fourier (second row) spectral methods when applied to the two-dimensional GPE (2) with $\vartheta = 100$.

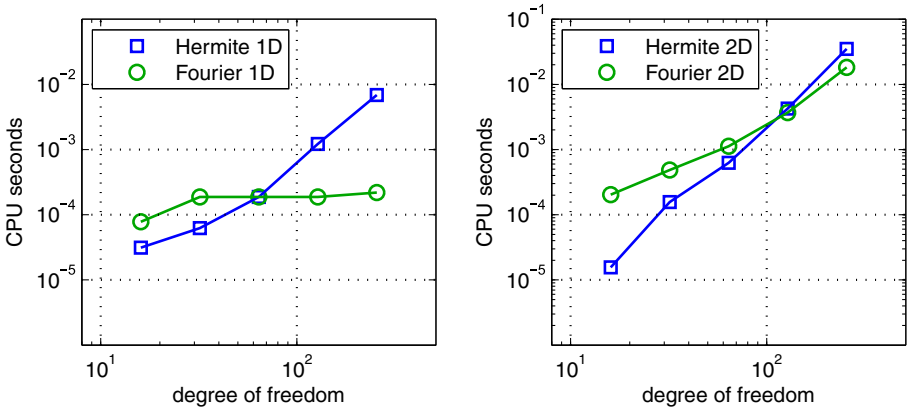

Fig. 6. Computation time of the Hermite and Fourier spectral methods in one (left picture) and two (right picture) space dimensions.

SRKN_{14}^{a} with 128×128 degrees of freedom and a temporal step size corresponding to $N = 2^{17}$ time steps. For different combinations of degrees of freedom and temporal step sizes, constrained to be equal to powers of two, we compute the global error in the L^2-norm and the total number of spectral transformations; further, we measure the particle number (3a) and energy (3b) conservation with respect to the initial values. Prescribing certain tolerances for the global discretisation error, the optimal performances corresponding to the smallest values of the required degrees of freedom and the number of spectral transformations are displayed in Table 2.

In the present situation, for any time integration method, the number of basis functions required for the Hermite spectral method is always smaller than the number of basis functions required for the Fourier spectral method; moreover, in many cases, the number of Hermite spectral transformations is smaller than the number of Fourier spectral transformations. This observation is in accordance with Figs. 2 and 4 showing that the Hermite spectral method is slightly more accurate. Comparing the time-splitting methods, the fourth and sixth-order schemes, which behave in a similar manner, require less spectral transformations than the second-order Strang splitting and thus are more efficient; moreover, for the Strang splitting, it was not possible to reach a tolerance smaller than 10^{-4} within the maximal number of 2^{15} timesteps. For each time-splitting spectral method, the particle number and the energy are well preserved.

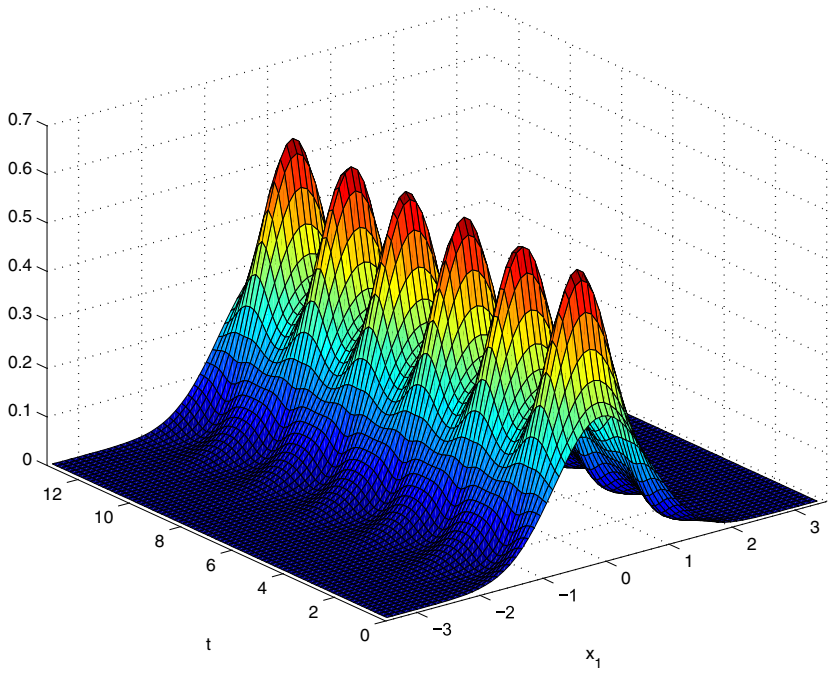

Fig. 7. Numerical solution $\psi(x_1, 0, t)$ of the GPE ("breathing") for $\vartheta = 1$ up to a final time $T = 13$. Slice along $x_2 = 0$.

Table 2
Time integration of the GPE ("breathing") with $\vartheta = 1$ up to $T = 400$. For a tolerance (Tol.), the degree of freedom (D.o.f.), the number of transformations (#Transf.), the particle number conservation error ($\Delta_{\text{pn}} = |\,\|\psi(\cdot,0)\|_{L^2}^2 - \|\psi(\cdot,T)\|_{L^2}^2\,|$), and the energy conservation error ($\Delta_E = |E(\psi(\cdot,0)) - E(\psi(\cdot,T))|$) are reported.

Tol.	M	D.o.f.	#Transf.	Δ_{pn}	Δ_E
$< 10^{-2}$	Hermite 2	32×32	16384	$2.6 \cdot 10^{-11}$	$4.2 \cdot 10^{-6}$
$< 10^{-2}$	Fourier 2	64×64	32768	$3.6 \cdot 10^{-13}$	$1.6 \cdot 10^{-6}$
$< 10^{-2}$	Hermite 4	32×32	6144	$9.7 \cdot 10^{-12}$	$1.1 \cdot 10^{-5}$
$< 10^{-2}$	Fourier 4	64×64	12288	$1.7 \cdot 10^{-13}$	$9.1 \cdot 10^{-7}$
$< 10^{-2}$	Hermite 6	32×32	14337	$2.3 \cdot 10^{-11}$	$3.2 \cdot 10^{-8}$
$< 10^{-2}$	Fourier 6	64×64	7169	$1.1 \cdot 10^{-13}$	$6.8 \cdot 10^{-6}$
$< 10^{-2}$	Hermite rk4	32×32	65532	$2.1 \cdot 10^{-5}$	$1.2 \cdot 10^{-4}$
$< 10^{-2}$	Fourier rk4	64×64	524284	$6.4 \cdot 10^{-10}$	$3.7 \cdot 10^{-9}$
$< 10^{-2}$	Hermite ode45	32×32	208376	$2.6 \cdot 10^{-8}$	$1.5 \cdot 10^{-7}$
$< 10^{-2}$	Fourier ode45	64×64	1132436	$5.6 \cdot 10^{-12}$	$3.1 \cdot 10^{-11}$
$< 10^{-4}$	Hermite 4	32×32	12288	$1.9 \cdot 10^{-11}$	$2.6 \cdot 10^{-9}$
$< 10^{-4}$	Fourier 4	128×128	12288	$1.6 \cdot 10^{-12}$	$1.8 \cdot 10^{-9}$
$< 10^{-4}$	Hermite 6	32×32	14337	$2.3 \cdot 10^{-11}$	$3.2 \cdot 10^{-8}$
$< 10^{-4}$	Fourier 6	128×128	14337	$2.0 \cdot 10^{-12}$	$2.5 \cdot 10^{-8}$
$< 10^{-4}$	Hermite rk4	32×32	131068	$6.5 \cdot 10^{-7}$	$3.8 \cdot 10^{-6}$
$< 10^{-4}$	Fourier rk4	128×128	524284	$6.4 \cdot 10^{-10}$	$3.7 \cdot 10^{-9}$
$< 10^{-4}$	Hermite ode45	32×32	208376	$2.6 \cdot 10^{-8}$	$1.5 \cdot 10^{-7}$
$< 10^{-4}$	Fourier ode45	128×128	1411226	$1.3 \cdot 10^{-9}$	$9.4 \cdot 10^{-7}$
$< 10^{-6}$	Hermite 4	64×64	24576	$1.0 \cdot 10^{-10}$	$1.1 \cdot 10^{-10}$
$< 10^{-6}$	Fourier 4	128×128	49152	$6.7 \cdot 10^{-12}$	$1.2 \cdot 10^{-11}$
$< 10^{-6}$	Hermite 6	64×64	28673	$1.2 \cdot 10^{-8}$	$2.1 \cdot 10^{-10}$
$< 10^{-6}$	Fourier 6	128×128	28673	$4.2 \cdot 10^{-12}$	$8.7 \cdot 10^{-12}$
$< 10^{-6}$	Hermite rk4	64×64	524284	$6.4 \cdot 10^{-10}$	$3.7 \cdot 10^{-9}$
$< 10^{-6}$	Fourier rk4	128×128	524284	$6.4 \cdot 10^{-10}$	$3.7 \cdot 10^{-9}$
$< 10^{-6}$	Hermite ode45	64×64	509816	$3.6 \cdot 10^{-10}$	$2.1 \cdot 10^{-9}$
$< 10^{-6}$	Fourier ode45	128×128	1411448	$2.2 \cdot 10^{-12}$	$1.1 \cdot 10^{-11}$

We also performed this long-term integration using two standard explicit methods; we chose a constant step size Runge–Kutta method of order four, see also Dion and Cancès [11], and further the adaptive Runge–Kutta method by Dormand and Prince implemented in the MATLAB-routine `ode45`. As the stiffness of the problem restricts the maximal temporal step size, the time-splitting methods outperform the explicit Runge–Kutta methods.

For larger values of ϑ, additional experiments not reported here showed that the Fourier spectral method becomes favourable; moreover, smaller time step sizes are required in order to reach the prescribed tolerances, see also Section 5.1. The influence of ϑ on the convergence behaviour of time-splitting spectral methods should be investigated further.

6. Conclusions and future work

We devoted the present paper to high-accuracy discretisations of the time-dependent GPE (2), based on Hermite and Fourier pseudospectral methods and exponential operator splitting methods. In particular, we presented numerical comparisons regarding accuracy and efficiency. In most of our experiments, we used the ground state solution of (2) as a reliable reference solution.

As expected, our numerical experiments showed that the spectral methods perform well regarding accuracy, efficiency, and the preservation of geometric properties. For the time integration we compared the second order Strang splitting with fourth and sixth-order splitting methods given in Blanes and Moan [5]; the higher-order schemes proved to be superior when low tolerances are required or a long-term integration is carried out. Furthermore, each time-splitting method outperformed the explicit Runge–Kutta methods in the "breathing" experiment.

Following [17,26], it remains open to provide a stability and convergence analysis for high-order exponential operator splitting methods when applied to the time-dependent GPE (2). Furthermore, it is of interest to investigate the accuracy of time-splitting methods when the nonlinear part increases.

References

[1] W. Bao, D. Jaksch, P. Markowich, Numerical solution of the Gross–Pitaevskii equation for Bose–Einstein condensation, J. Comp. Phys. 187 (2003) 318–342.
[2] W. Bao, J. Shen, A fourth-order time-splitting Laguerre–Hermite pseudospectral method for Bose–Einstein condensates, SIAM J. Sci. Comput. 26/6 (2005) 2010–2028.
[3] W. Bao, W. Tang, Ground-state solution of Bose–Einstein condensate by directly minimising the energy functional, J. Comp. Phys. 187 (2003) 230–254.
[4] C. Besse, B. Bidégaray, S. Descombes, Order estimates in time of splitting methods for the nonlinear Schrödinger equation, SIAM J. Numer. Anal. 40/5 (2002) 26–40.
[5] S. Blanes, P.C. Moan, Practical symplectic partitioned Runge–Kutta and Runge–Kutta–Nyström methods, J. Comput. Appl. Math. 142 (2002) 313–330.
[6] J. Boyd, Chebyshev and Fourier Spectral Methods, second ed., Dover, New York, 2001.
[7] M. Caliari, G. Kirchner, M. Thalhammer, Convergence and energy conservation of the Strang time-splitting Hermite spectral method for nonlinear Schrödinger equations, Universität Innsbruck, 2007, Preprint.
[8] M. Caliari, A. Ostermann, S. Rainer, M. Thalhammer, A minimisation approach for computing the ground state of Gross–Pitaevskii systems, J. Comp. Phys., in press, doi:10.1016/j.jcp.2008.09.018.
[9] Th. Cazenave, An Introduction to Nonlinear Schrödinger Equations, Textos de Métodos Matemáticos 26, I.M.U.F.R.J., Rio de Janeiro, 1989.
[10] E. Celledoni, D. Cohen, B. Owren, Symmetric exponential integrators for the cubic Schrödinger equation, Preprint Numerics 3/2006, University of Trondheim, 2006.
[11] C.M. Dion, E. Cancès, Spectral method for the time-dependent Gross–Pitaevskii equation with a harmonic trap, Phys. Rev. E 67 (2003) 046706.
[12] W. Gautschi, Orthogonal Polynomials: Computation and Approximation, Oxford University Press, Oxford, 2004.
[13] W. Gautschi, Orthogonal polynomials (in Matlab), J. Comput. Appl. Math. 178 (2005) 215–234.
[14] E.P. Gross, Structure of a quantized vortex in boson systems, Nuovo. Cimento. 20 (1961) 454–477.
[15] E. Hairer, Ch. Lubich, G. Wanner, Geometric Numerical Integration. Structure-Preserving Algorithms for Ordinary Differential Equations, Springer, Berlin, 2002.
[16] W. Kahan, R.-C. Li, Composition constants for raising the orders of unconventional schemes for ordinary differential equations, Math. Comput. 66 (1997) 1089–1099.
[17] Ch. Lubich, On splitting methods for Schrödinger–Poisson and cubic nonlinear Schrödinger equations, Math. Comp. 77/264 (2008) 2141–2153.
[18] R.I. McLachlan, On the numerical integration of ordinary differential equations by symmetric composition methods, SIAM J. Sci. Comput. 16 (1995) 151–168.
[19] R.I. McLachlan, R. Quispel, Splitting methods, Acta Numer. 11 (2002) 341–434.
[20] V.M. Pérez–García, X. Liu, Numerical methods for the simulation of trapped nonlinear Schrödinger systems, Appl. Math. Comp. 144 (2003) 215–235.
[21] L.P. Pitaevskii, Vortex lines in an imperfect Bose gas, Sov. Phys. JETP 13 (1961) 451–454.
[22] G. Strang, On the construction and comparison of difference schemes, SIAM J. Numer. Anal. 5 (1968) 506–517.
[23] M. Suzuki, Fractal decomposition of exponential operators with applications to many-body theories and Monte Carlo simulations, Phys. Lett. A 146 (1990) 319–323.
[24] Y.-F. Tang, L. Vázquez, F. Zhang, V.M. Pérez–García, Symplectic methods for the nonlinear Schrödinger equation, Comput. Math. Appl. 32/5 (1996) 73–83.
[25] T.R. Taha, M.J. Ablowitz, Analytical and numerical aspects of certain nonlinear evolution equations. II. Numerical, nonlinear Schrödinger equation, J. Comput. Phys. 55/2 (1984) 203–230.
[26] M. Thalhammer, High-order exponential operator splitting methods for time-dependent Schrödinger equations, SIAM J. Numer. Anal. 46/4 (2008) 2022–2038.
[27] H.F. Trotter, On the product of semi-groups of operators, Proc. Am. Math. Soc. 10 (1959) 545–551.
[28] H. Yoshida, Construction of higher order symplectic integrators, Phys. Let. A 150 (1990) 262–268.